Available online at www.sciencedirect.com
ScienceDirect
Signal Processing 88 (2008) 1152–1164
SIGNAL PROCESSING
www.elsevier.com/locate/sigpro

Experimental antenna array calibration with artificial neural networks

Hugo Bertrand*, Dominic Grenier, Sébastien Roy

Department of Electrical and Computer Engineering, Université Laval, Que., Canada G1K 7P4

Received 23 August 2006; received in revised form 12 October 2007; accepted 7 November 2007
Available online 28 November 2007

Abstract

It is well known that to perform accurate Direction of Arrivals (DOA) estimation using algorithms like MUSIC (MUltiple SIgnals Classification), antenna array data must be calibrated to match the theoretical model upon which DOA algorithms are based. This paper presents experimental measurements from independent sources obtained with a linear antenna array and proposes a novel calibration technique based on artificial neural networks trained with experimental and theoretical steering vectors. In this context, the performance of 3 types of neural networks—ADAptive LInear Neuron (ADALINE) network, Multilayer Perceptrons (MLP) network and Radial Basis Functions (RBF) network—is assessed. This is then compared with other calibration techniques, thus demonstrating that the proposed technique works well while being very simple to implement. The presented results cover operation with a single signal source and with two uncorrelated sources. The proposed method is applicable to arbitrary array topologies, but is presented herein in conjunction with a uniform linear array (ULA).

Keywords: Antenna arrays; Calibration; Artificial neural networks; Array processing; Beamforming; DOA; MUSIC

1. Introduction

Array antenna usage in various communication, radar and instrumentation systems has been growing dramatically over the last few years for several reasons. The emergence of new antenna shapes simplified their production, given their simplicity. Several such antennas can be integrated, together with some circuitry, into a monolithic small-scale device, effectively resulting in low-cost, diminutive antenna arrays. The advent of increasingly cheaper signal processing chips (DSP) makes possible the sophisticated processing of the plurality of signals from an antenna array at a low-cost, low-power consumption, and in a small form factor. Given the digital processing power available to analog to digital interface can be moved closer to the antenna, thus reducing the complexity and cost of the RF section. This core signal processing itself can take various forms, can include parameter estimation, adaptive filtering and detection.

In the case of this present work, two well-known classes of space-time processing algorithms are of interest: beamforming and Direction of Arrivals (DOA) estimation.

*Corresponding author
E-mail addresses: hbertran@gel.ulaval.ca, hugo.bertrand.1@ulaval.ca (H. Bertrand), dgrenier@gel.ulaval.ca (D. Grenier), sebasroy@gel.ulaval.ca (S. Roy).

0165-1684/$ - see front matter © 2007 Elsevier B.V. All rights reserved.
doi:10.1016/j.sigpro.2007.11.006

However, in a real-world, there are some reasons which limit the general use of antenna arrays. One of them is the precise calibration required such arrays when they are used for specific tasks, such as beamforming and DOA estimation which require the acquisition of the precise amplitude and phase relationships of the signals collected at each element. These relations are unfortunately sensitive to many potential error sources, leading to severe performance constraints. First, phase and gain imbalances between the in-phase (I) and quadrature (Q) branches of each element receiver/transmitter subsystem and the I/Q bias errors due to electronic DC offsets cause a divergence from the statistical model upon which signal processing algorithms depend; more details on this source of error are available in [1,2]. Indeed, the said algorithms are constructed based on various assumptions, such as the ideal properties of complex Gaussian variates originally postulated by Goodman [3]. Another deviation between theory and practice is due to the co-channel gain and phase errors, i.e. the variations between the multiple element receiver/transmitter subsystems themselves. The third error source is the mutual coupling effects between the elements comprising the array. The fourth error source in an experimental antenna array setup is the element location errors or uncertainties. Finally, scattering by the antenna mounting structure or other nearby structures constitutes a fifth source. These causes of errors can be considered statics during a sufficient period of time.

All of these perturbations consequently affect the specific structure of the data covariance matrix. Furthermore, the theoretical steering vectors can find themselves outside the experimental signal subspace. These effects imply a poor or erroneous performance by signal processing algorithms, as can be seen in Section 5 and in [4,5] which analyze the performance of these algorithms in the presence of model errors.

The solution to all of these problems is inevitably some form of data calibration to fit the theoretical model or, equivalently, the experimental array manifold calibration with respect to the presumed steering vectors set. Fig. 1 shows a schematic representation of a linear uniformly spaced antenna array used to perform DOA estimation for M sources. The RF front-end is detailed in Section 5 while the digital processing apparatus is discussed in Sections 2 and 4.

A lot of contributions can be found in the literature on the topic of antenna array calibration. Most

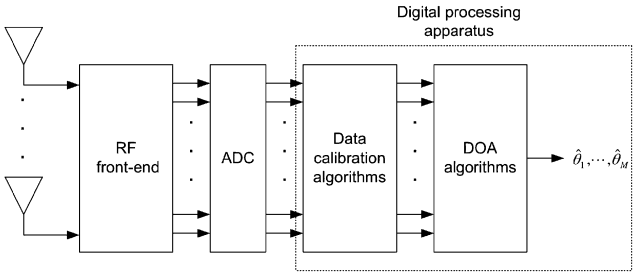

Fig. 1. A schematic representation of a linear equispaced array receiver performing DOA estimation.

are based only on simulation, which by itself probably yields an incomplete picture of this essentially experimental issue. These works can collectively be slated into three main approaches. First, some authors [6] attempt to bypass the calibration problem by constructing a new data covariance matrix which has a Toeplitz structure. The second class is referred to as *auto calibration* or *online calibration*, because it does not require knowledge of the directions of the calibrating sources. Finally, the last approach is designated *trained calibration* or *offline calibration* and it implies knowledge of the calibrating sources' (pilots) exact bearings.

The first approach is only applicable in the case where sensor location errors alone are present. The second one is generally iterative and is not really self-sufficient, because such algorithms, globally based on some form of least-squares fit, require initial calibration [7–12], some a priori information about a received signal (such as a CDMA code [7,8]) and/or it is assumed that part of the response is known (like in [13] where the sensor gains are assumed known). Also, these iterative algorithms can potentially converge to a local minimum rather than the global one if the initial conditions are not sufficiently close to the solution [7,10,14–16]. Furthermore, the majority of these pseudo-self-calibration algorithms have been studied by focusing on one or more error sources, but rarely on all. For example, [12,17–20] focus only on the amplitude and/or phase errors, [21] on mutual coupling and scattering, [22–25] on I/Q imbalances and [15,26] on sensor position errors or uncertainties. Also, some techniques [27,28] necessitate a different calibration step for each error source.

On the other hand, training-based calibration requires knowledge of the calibrating sources' angular positions [4,12,14,29–32]. As explained

previously, however, these self-calibration algorithms are also heavily dependent on various idealizations.

So, the concept of supervised calibration online is investigated and it is found that artificial neural networks (ANNs) constitute a powerful algorithmic tool for this application. In the literature, the joint use of neural networks and antenna arrays serves almost exclusively to directly estimate the directions of arrivals of signals impinging on the array [33,34]. The principal advantage of neural networks over classical DOA algorithms is that they can learn from non-calibrated data (calibration is implicit to the learning process), but the training procedure for more than one source is in our view too demanding (i.e. the number of training samples grows in a combinatorial fashion with the number of sources) for a practical implementation [35] and this is why in previous efforts such as [36] experiments are limited to the one source case. To the best of the authors' knowledge, there is only two papers which performs explicit antenna array calibration via neural networks [37,39], but it provides no details on the data used to train the network and no explicit results of the calibration or comparisons with other algorithms. Furthermore, the neural network selected comprises many neurons and the training algorithm, a variation of the backpropagation algorithm, seems heavy for this problem, leading to significant implementation complexity.

The above observation is based on the fact that our implementation gives excellent experimental results even though it is based on a single-layer linear neural network comprising far fewer neurons than the solution presented in [37]. Furthermore, it is trained with the experimental and theoretical steering vectors by a low-complexity algorithm based on least-squares optimization. This simplicity makes the proposed algorithm an ideal candidate for real-time low-cost implementation. It should also be noted that, although the experimental array used herein is of the uniform linear (ULA) variety, this is not restrictive and the proposed method can be applied to any topology.

The paper is organized as follows: Section 2 describes the antenna array model; Section 3 introduces the ANN model; Section 4 describes the proposed algorithms as well as two other algorithms often seen in the literature for comparison and Section 5 presents the experimental setup and results. Finally, Section 6 concludes the paper by discussing and summarizing the findings.

2. Antenna array model

We consider here an N-sensor uniform linear array (ULA) with I/Q receivers at each sensor as seen in Fig. 2, but any other N-sensor array geometry can be used. The output of the nth sensor is formed by the in-phase I_n and the out-of-phase Q_n components of the received signal. From sampling all receiver outputs, we build the matrix $\mathbf{X}$ composed by K independent snapshot vectors $\mathbf{x}_k$. We can assume that a snapshot comprises N Gaussian random components of the Goodman class [3] with zero-mean and covariance matrix $\mathbf{R}$. This distribution originates in part from the fact that the signals emitted by the M sources are independent (and hence uncorrelated). It is also based on the assumption of independent Gaussian samples which is widely used in signal processing [38, Appendix J] and is known to work well when applied to linear systems.

Each of these snapshot vectors can be expressed as

$$\begin{aligned}\mathbf{x}_k &= [(I_1 + \mathrm{j}Q_1)(I_2 + \mathrm{j}Q_2)\cdots(I_N + \mathrm{j}Q_N)]^{\mathrm{T}} \\ &= \sum_{i=1}^{M} \alpha_i(k)\mathbf{a}(\theta_i) + \boldsymbol{\eta}_k, \end{aligned} \tag{1}$$

where $\alpha_i(k)$ are complex random Gaussian variables with zero-mean and variance σ_i^2 related to the power received from the ith source, $\mathbf{a}(\theta_i)$ are the steering vectors associated with the ith source and $\boldsymbol{\eta}_k$ are vectors of zero-mean additive Gaussian noise with variance σ_η^2.

For a ULA, the steering vector of the ith source is theoretically given by

$$\mathbf{a}(\theta_i) = \frac{1}{\sqrt{N}}[1 \;\; \mathrm{e}^{\mathrm{j}\varphi_i} \;\; \mathrm{e}^{\mathrm{j}2\varphi_i} \;\; \cdots \;\; \mathrm{e}^{\mathrm{j}(N-1)\varphi_i}]^{\mathrm{T}}, \tag{2}$$

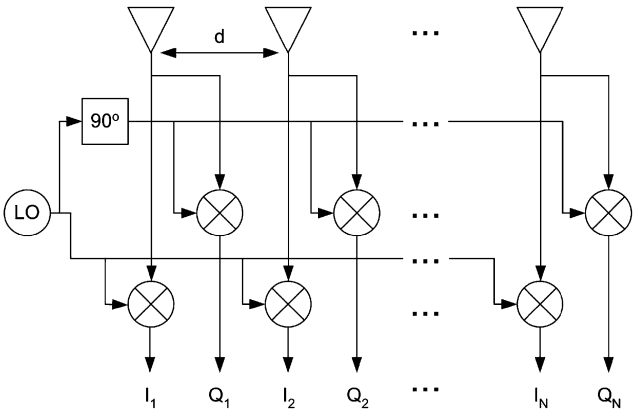

Fig. 2. A linear equispaced array.

where φ_i is the electrical delay between each antenna's signal due to the inter-antenna distance d, the ith source's position θ_i and his wavenumber λ_i and is expressed

$$\varphi_i = \frac{2\pi d}{\lambda_i}\sin(\theta_i). \tag{3}$$

The data matrix can now be expressed as

$$\begin{aligned}\mathbf{X} &= [\mathbf{x}_1\ \mathbf{x}_2\ \cdots\ \mathbf{x}_K] \\ &= \mathbf{AS} + \mathbf{N},\end{aligned} \tag{4}$$

with

$$\mathbf{A} = [\mathbf{a}(\theta_1)\ \mathbf{a}(\theta_2)\ \cdots\ \mathbf{a}(\theta_M)], \tag{5}$$

$$\mathbf{N} = [\boldsymbol{\eta}_1\ \boldsymbol{\eta}_2\ \cdots\ \boldsymbol{\eta}_K], \tag{6}$$

$$\mathbf{S} = [\mathbf{s}_1\ \mathbf{s}_2\ \cdots\ \mathbf{s}_K], \tag{7}$$

$$\mathbf{s}_k = [\alpha_1(k)\ \alpha_2(k)\ \cdots\ \alpha_M(k)]^{\mathrm{T}}. \tag{8}$$

In this ideal situation, the data covariance matrix $\mathbf{R}$ is Hermitian Toeplitz and can be approximated by

$$\hat{\mathbf{R}} \approx \mathbf{X}\mathbf{X}^{\mathrm{H}}, \tag{9}$$

where $\langle\bullet\rangle^{\mathrm{H}}$ denotes the complex conjugate transpose operation. We can perform its eigendecomposition:

$$\begin{aligned}\mathbf{R} &= \sum_{i=1}^{M}\lambda_i\mathbf{v}_i\mathbf{v}_i^{\mathrm{H}} + \sum_{i=M+1}^{N}\lambda_i\mathbf{v}_i\mathbf{v}_i^{\mathrm{H}} \\ &= \mathbf{V}_{\mathrm{s}}\boldsymbol{\Lambda}_{\mathrm{s}}\mathbf{V}_{\mathrm{s}}^{\mathrm{H}} + \sigma_\eta^2\mathbf{I},\end{aligned} \tag{10}$$

where $\{\lambda_i\}$ are the N eigenvalues in decreasing magnitude order, associated with the eigenvectors $\{\mathbf{v}_i\}$. The Hermitian symmetry of this matrix ensures that the eigenvalues are real and the eigenvectors are orthogonal. The first M eigenvectors constitute the signal subspace and the others form the noise subspace.

We know that the M first eigenvectors span the same subspace as the M assumed steering vectors $\mathbf{a}(\theta_1)$ to $\mathbf{a}(\theta_M)$ and the other eigenvectors define a subspace orthogonal to the steering vectors.

This structure is exploited by classic DOA algorithms. For example, the MUSIC (MUltiple SIgnals Classification) algorithm [40] is based on the ordinary Euclidian distance between all the possible steering vectors and the signal subspace and can be expressed as

$$P_{\mathrm{music}}(\theta) = 20\log_{10}\left(\frac{1}{\mathbf{a}^{\mathrm{H}}(\theta)\mathbf{P}_n\mathbf{a}(\theta)}\right), \tag{11}$$

where $\mathbf{a}(\theta)$ is built like (2) using θ as a scanning angle variable and $\mathbf{P}_n = \mathbf{I} - \mathbf{V}_{\mathrm{s}}\mathbf{V}_{\mathrm{s}}^{\mathrm{H}}$ is the projector to the noise subspace which is perpendicular to the signal subspace spanned by the eigenvectors $\mathbf{V}_{\mathrm{s}}$. Eq. (11) is called the MUSIC pseudospectrum.

Unfortunately, when experimental data from an uncalibrated array are used with this algorithm, it yields erroneous results (as can be seen in Fig. 13). This is due to the fact that the theoretical steering vectors do not lie exactly in the experimental signal subspace. It follows that we have to modify the underlying theoretical model to take into account the effects of the non-ideal behavior of the experimental antenna array.

Based on the simplifying assumption that the problem is linear, the experimental data matrix collected from an experimental uncalibrated antenna array is now given by

$$\mathbf{X} = \boldsymbol{\Gamma}\mathbf{AS} + \mathbf{N}, \tag{12}$$

where $\boldsymbol{\Gamma}$ is a complex distortion square matrix which embodies all the non-ideal effects due to imperfections in the experimental array. If the array presents only gain and phase errors between the I and Q branches of each sensor, $\boldsymbol{\Gamma}$ is diagonal. In the cases of branch-to-branch gain and phase mismatches and mutual coupling, $\boldsymbol{\Gamma}$ includes off-diagonal elements. Sensor location errors can also be taken into account, since they constitute another source of branch-to-branch gain and phase errors. It follows that all non-ideal effects of the experimental setup can be encapsulated in this distortion matrix.

Hence, the goal of the calibration procedure is to compensate for the distortion matrix—which embodies all linear imperfections—in addition to any non-linear distortions which might be present.

3. ANN model

ANNs are used herein as a distributed parallel computing mechanism which establishes a mapping between the input and output spaces of the network, like a lookup table with intrinsic interpolation between samples. This mapping is constructed implicitly via supervised learning, i.e. the presentation to the network of training samples comprising an input signal and a corresponding desired response. During training, the values of weights and biases are modified to minimize the error between the output of the network and the desired one until the network converges to a steady state.

Fig. 3 presents the model of an ANN with two layers in matrix notation. The network output $\mathbf{y}^2$ is

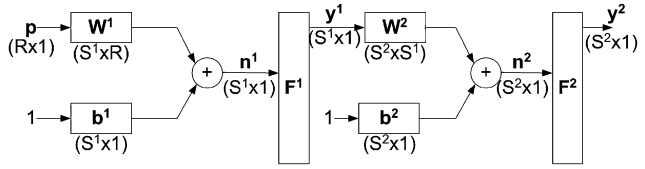

Fig. 3. ANN model.

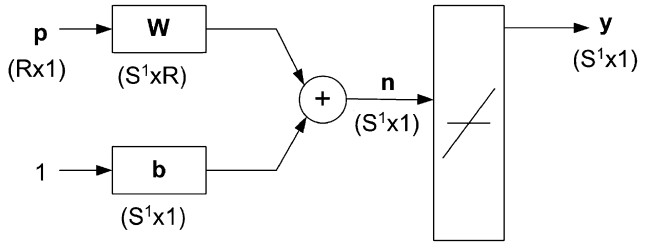

Fig. 4. ADALINE neural network mdel.

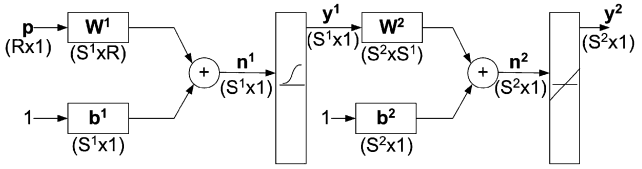

Fig. 5. MLP neural network model.

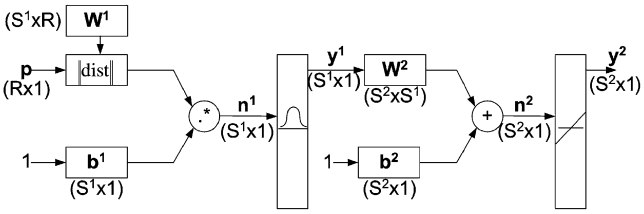

Fig. 6. RBF neural network model.

linked to the input $\mathbf{p}$ via

$$\mathbf{y}^2 = \mathbf{F}^2(\mathbf{n}^2) = \mathbf{F}^2(\mathbf{W}^2[\mathbf{F}^1(\mathbf{W}^1\mathbf{p} + \mathbf{b}^1)] + \mathbf{b}^2), \tag{13}$$

where $\{\mathbf{W}^i\}$ are the weight matrices, $\{\mathbf{b}^i\}$ the bias vectors, $\{\mathbf{y}^i\}$ the output vectors and $\mathbf{F}^i$ are the activation functions of the ith layer.

The proposed calibration technique has been implemented with different types of ANNs, i.e. ADAptive LInear NEuron (ADALINE), Multilayer Perceptrons (MLP) and Radial Basis Functions (RBF). The simplest type of neural network used is ADALINE [41], which consists of a single layer and a linear activation function as illustrated in Fig. 4.

The supervised training of this network is based on an approximation of the minimization of the sum of the squared errors between the outputs of the network and the desired responses, as described in Section 4.2.

The output $\mathbf{y}$ of this network is obtained with

$$\mathbf{y} = \mathbf{W}\mathbf{p} + \mathbf{b}. \tag{14}$$

The second type of neural network used is a form of MLP which consists of two neuron layers, the first one having a logsigmoid activation function

$$F^1 = \mathrm{logsig}(n) = \frac{1}{1 + \mathrm{e}^{-n}}, \tag{15}$$

and the second one having the linear activation function illustrated in Fig. 5. The weights and biases of the network are iteratively adjusted to minimize the network performance function, i.e. the average squared error between the network outputs and the target outputs. This iterative training procedure is performed using the backpropagation algorithm [42] which uses the negative of the gradient of the performance function to update the values of biases and weights at each iteration.

The output $\mathbf{y}^2$ of this network is obtained with

$$\mathbf{y}^2 = \mathbf{W}^2\mathbf{y}^1 + \mathbf{b}^2 = \mathbf{W}^2\,\mathrm{logsig}(\mathbf{W}^1\mathbf{p} + \mathbf{b}^1) + \mathbf{b}^2. \tag{16}$$

The third neural network used to perform the calibration procedure is an RBF comprising two layers of neurons. The first one is composed of radial basis functions

$$F^1 = \mathrm{radbas}(n) = \mathrm{e}^{-n^2}, \tag{17}$$

and the second one of linear activation functions, as illustrated in Fig. 6. The training procedure of this network is quite different from the others: the weights of the first layer are fixed to the values of the training patterns, the biases are all equal to a constant value determined by

$$\mathbf{b}^1 = \frac{0.8326}{\mathrm{SPREAD}}, \tag{18}$$

where SPREAD is a numerical value found empirically which determines the width of an area in the input space to which each neuron responds. The second layer is trained in a manner identical to the ADALINE network. The output $\mathbf{y}^2$ of this network is obtained with

$$\mathbf{y}^2 = \mathbf{W}^2\mathbf{y}^1 + \mathbf{b}^2 = \mathbf{W}^2\,\mathrm{radbas}(\|\mathbf{W}^1 - \mathbf{p}\| \circ \mathbf{b}^1) + \mathbf{b}^2, \tag{19}$$

where $\|\mathbf{W}^1 - \mathbf{p}\|$ is the Euclidean distance between each rows of $\mathbf{W}^1$ and $\mathbf{p}$, and $\circ$ is the Hadamard product.

The choice of the ADALINE neural network is motivated by its simplicity and relies on the linear assumption discussed earlier. The MLP structure is drawn from [37] where it is used for calibration purposes and serves as a performance benchmark. Indeed, it constitutes a rare example of a published application of neural networks to the calibration problem. Finally, the RBF neural network is included because it can be quickly and easily designed and constitutes a natural solution in a mapping application between the input and output spaces of the network. Both the MLP and RBF networks perform non-linear processing (which implies higher complexity) and can therefore help to determine whether the linear assumption is justified.

For further details on the neural network models and associated learning algorithms, see [41–43].

4. Calibration algorithms

In what follows, we review existing algorithms before presenting the proposed algorithm in relation with the state of the art.

4.1. Known algorithms used for comparison

As stated previously, the theoretical steering vectors $\mathbf{a}(\theta_i)$ do not lie completely in the experimental signal subspace without calibration. Most previous works (see for example [14]) propose to find a calibration matrix $\mathbf{G}$, it being the inverse of $\mathbf{\Gamma}$ in (12) in the least-squares sense. Mathematically, we have

$$\hat{\mathbf{G}} = \min_{\mathbf{G}} \|\mathbf{A} - \mathbf{G}\hat{\mathbf{A}}_e\|, \tag{20}$$

where $\hat{\mathbf{A}}_e$ denotes an estimate of the experimental steering vectors obtained via eigenanalysis of the spatial covariance data matrix. The matrix $\mathbf{A}$ is the theoretical one obtained from (2) given the exact position of sources.

The minimization (20) can be solved to yield [42]:

$$\hat{\mathbf{G}} = \mathbf{A}(\hat{\mathbf{A}}_e^{\mathrm{H}}\hat{\mathbf{A}}_e)^{-1}\hat{\mathbf{A}}_e^{\mathrm{H}}. \tag{21}$$

The calibration procedure is then simply

$$\mathbf{Y} = \hat{\mathbf{G}}\mathbf{X}, \tag{22}$$

where $\mathbf{Y}$ is the calibrated data matrix. The major problem with this method is the possibility of convergence to a local minimum rather than the global one.

Another calibration algorithm [22], which corrects only I/Q imbalances, is based on the principle of the Gram–Schmidt orthogonalization. Consider the in-line I_i and quadrature Q_i signals at each antenna

$$\begin{aligned} I_i(t) &= (1+\varepsilon)A\cos(\omega t) + \varepsilon_I, \\ Q_i(t) &= A\sin(\omega t + \phi) + \varepsilon_Q, \end{aligned} \tag{23}$$

where ε represents the amplitude difference between these components, ε_I and ε_Q the signal offsets and ϕ the phase imbalance between them. First of all, the DC offsets ε_I and ε_Q must be removed to obtain new signals I_i' and Q_i'

$$\begin{aligned} I_i'(t) &= (1+\varepsilon)A\cos(\omega t), \\ Q_i'(t) &= A\sin(\omega t + \phi). \end{aligned} \tag{24}$$

By virtue of the Gram–Schmidt procedure, a scalar E must be found to normalize I_i' and a part P of I_i' must be subtracted from Q_i' to complete the orthogonalization and finally obtain signals I_i'' and Q_i''. In matrix notation, we have

$$\begin{bmatrix} I_i''(t) \\ Q_i''(t) \end{bmatrix} = \begin{bmatrix} E & 0 \\ P & 1 \end{bmatrix} \begin{bmatrix} I_i'(t) \\ Q_i'(t) \end{bmatrix}.$$

The desired result being

$$\begin{aligned} &\|I_i''(t)\| = \|Q_i''(t)\|, \\ &\frac{I_i''(t)}{Q_i''(t)} = \mathrm{e}^{\pm \mathrm{j}\frac{\pi}{2}}, \end{aligned} \tag{25}$$

we find after some algebraic manipulations

$$\begin{aligned} E &= \frac{\cos(\phi)}{1+\varepsilon}, \\ P &= \frac{-\sin(\phi)}{1+\varepsilon}. \end{aligned} \tag{26}$$

The major advantage of this technique is its autonomy, i.e. it does not rely on a set of known sources for training purposes. Hence, it can be referred to as *absolute calibration*; its performance, however, is poor compared to our expectation as illustrated in Section 5.

4.2. Proposed algorithm

The originality of the proposed approach centers on the use of ANNs to perform calibration. ANNs can easily provide real-time solutions thanks to their relatively low computational complexity and their mostly parallel architecture which makes them natural candidates for implementation in VLSI [44–46]. Experiments have shown that they also

alleviate the problem of convergence to a local minimum since they typically always converge to the global one when training and structure are adequate. We find that a linear neural network trained with L input/target vector pairs formed by the real and imaginary parts of the experimental and assumed steering vectors gives excellent results even if the learning algorithm is very simple and the number of neurons is small.

Fig. 7 shows a block diagram overview of the DOA processing chain with the proposed calibration approach. It consists of the standard sequence of operations detailed in Section 2 which lead to the MUSIC pseudospectrum, with the inclusion at the front end of the neural network which compensates for all distortions by minimizing a single global quality measure, namely the mean-square error (MSE). *At first, we begin by the learning process which* adjusts the values of the weights and biases by minimizing an approximation of MSE between the output vectors $\mathbf{y}(k)$ ($\mathbf{a}_{\mathrm{cal}}(k)$, the calibrated steering vectors) and the target vectors $\mathbf{t}(k)$ ($\mathbf{a}(k)$, the exact steering vectors) for the input vectors $\mathbf{p}(k)$ ($\hat{\mathbf{a}}_{\mathrm{e}}(k)$, the experimental steering vectors), i.e.

$$\mathrm{MSE} = F(\mathbf{e}) \approx \frac{1}{L}\sum_{k=1}^{L}\sum_{i=1}^{2N}(\mathrm{e}_i(k))^2 = \frac{1}{L}\sum_{k=1}^{L}\mathbf{e}(k)^{\mathrm{T}}\mathbf{e}(k), \tag{27}$$

with $\mathbf{e}(k) = \mathbf{t}(k) - \mathbf{y}(k)$. This performance index F is a quadratic form which ensures the convergence of the training process to a global minimum (the quadratic error surface is monotonic), as confirmed by the experimental results. Using the LMS algorithm [43], which approximates the MSE-based steepest descent procedure by using the instantaneous squared error as an estimate of the MSE at each iteration, the rules to update the network parameters at iteration $k+1$ are

$$\begin{aligned}\mathbf{W}(k+1) &= \mathbf{W}(k) + 2\alpha\mathbf{e}(k)\mathbf{p}^{\mathrm{T}}(k),\\ \mathbf{b}(k+1) &= \mathbf{b}(k) + 2\alpha\mathbf{e}(k),\end{aligned} \tag{28}$$

where α is the step size which is empirically chosen to ensure convergence.

One source located at various known angles of arrival is used at this step. Then, only the eigenvector associated to the highest eigenvalue at the output of the eigendecomposition box $\mathbf{p}(k)$ (see Fig. 7) is taken for the training. This eigenvector is equivalent to the experimental steering vector of the source $\hat{\mathbf{a}}_{\mathrm{e}}(k)$ for each angle of arrival. The ANN adjusts its parameters to give a calibrated steering vector $\mathbf{a}_{\mathrm{cal}}(k)$ very close to the exact steering vector $\mathbf{a}(k)$.

The calibration based on the two other considered types of neural networks gives similar results while requiring longer training (MLP) or comprising more neurons (RBF), as detailed below.

Once the training is complete, the DOA processing can now be applied with unknown sources. In this step, all eigenvectors are putted in the input of the ANN to obtain calibrated eigenvectors. The M eigenvectors associated to the highest eigenvalues span the same signal space that one spanned by the corresponding calibrated steering vectors. So, we get $\mathbf{P}_{n_{\mathrm{cal}}}$ which is taken to compute the ordinary Euclidian distance as in (11).

5. Experimental setup and results

Fig. 8 shows the experimental antenna array comprising 8 horn antennas operating in the X band (8–12 GHz). While the design of this setup was as rigorous as possible, it presents all the imperfections discussed previously, i.e. phase and gain imbalances

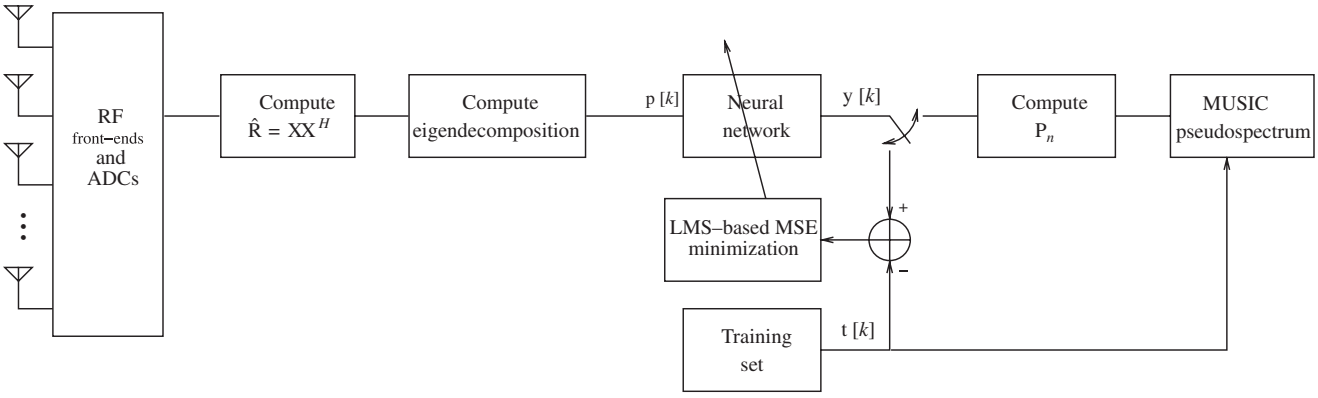

Fig. 7. Block diagram of DOA processing chain yielding MUSIC pseudospectrum (11) with neural network-based array calibration.

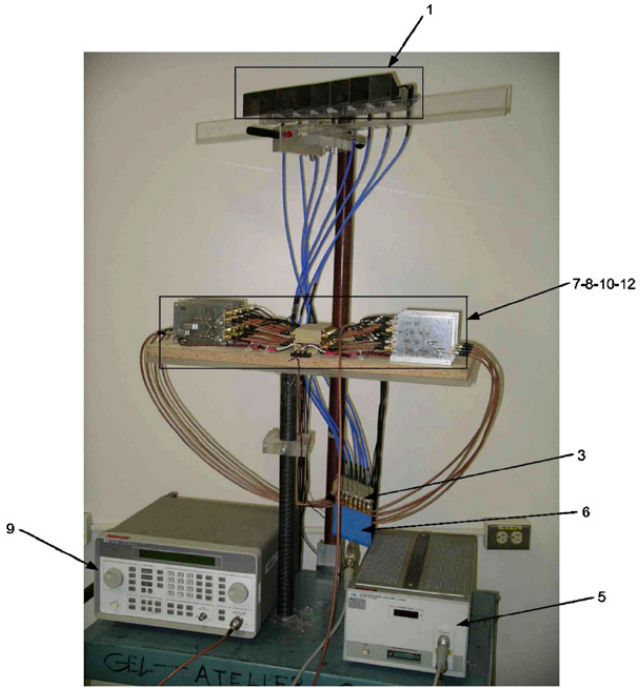

Fig. 8. The antenna array.

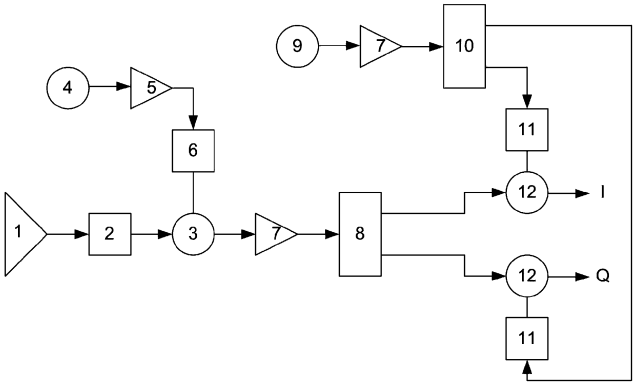

Fig. 9. Receiver chain block diagram in one antenna branch.

between the in-phase (I) and quadrature (Q) branches of each antenna receiver subsystem, I/Q bias errors, branch-to-branch gain and phase errors due to the variations between the antenna receiver subsystems, mutual coupling effects between the antennas on the array and sensor location errors or uncertainties and potentially scattering by the antenna mounting structure or other nearby structures.

The numbers in Fig. 8 refer to Fig. 9 which presents a block diagram of the experimental setup for a one-antenna receiver subsystem. The different elements are: 1. horn antenna, 2. waveguide WR-90 to SMA adaptor, 3. low noise RF amplifier and mixer, 4. RF generator, 5. RF amplifier, 6. power divider 1–8 (for each subsystem), 7. low frequency amplifier, 8. power divider 1–2 (for I/Q branches), 9. low frequency signal generator, 10. quadrature power divider, 11. power divider 1–8 (for each subsystem) and 12. low frequency mixer.

The effects of branch-to-branch gain and phase errors and sensor location errors are illustrated in Fig. 10.

Fig. 11 shows the calibration impact on signals with the proposed algorithm: branch-to-branch gain and phase errors are corrected, but it was observed that the calibration procedures do not alleviate completely the I/Q imbalances: the Lissajou I/Q plot [47] is still an ellipse as shown in Fig. 12 for a typical branch.

Finally, the compound effects of these perturbations on the performance of DOA algorithms is obvious when looking at Fig. 13, which presents the pseudospectra obtained before and after calibration for one source at 0°.

Given the effects of the imperfections of the experimental setup, details of the calibration procedure follow. Measurements are taken with one source in the X band at each half degree between −20° and 20°. For each measurement, the principal eigenvector of the spatial covariance matrix is used as the experimental steering vector, while the assumed steering vector is created based on the measured source position. This operation gives us the input/output training set.

Once the training set is obtained, the experimental steering vectors obtained from the users' signals can be calibrated to obtain their accurate DOAs.

Fig. 13 presents the excellent calibration result for one source at array broadside (0°) with a training with all sources. We can see that the best performance, the highest peak which corresponds to the shortest distance between the signal subspace and the calibration steering vector, is obtained by RBF, followed by MLP, ADALINE, **G** matrix and finally the I/Q calibration procedure. These results indicate that for a DOA in the training set, all trained algorithms give a good solution and we also conclude that the I/Q imbalances are less important for the performance of DOA algorithms than the branch-to-branch ones.

To compare the performance of these techniques when the DOA is not part of the training set, we calculate the mean angle θ_{average} between the calibrated $\mathbf{a}_{\text{cal}}$ and the theoretical $\mathbf{a}$ steering vectors for different sizes L of the training set

$$\theta_{\text{average}} = \frac{1}{L}\sum_{i=1}^{L} \arccos\left(\frac{\|\mathbf{a}^{\text{H}}(i)\mathbf{a}_{\text{cal}}(i)\|}{\|\mathbf{a}^{\text{H}}(i)\|\|\mathbf{a}_{\text{cal}}(i)\|}\right). \tag{29}$$

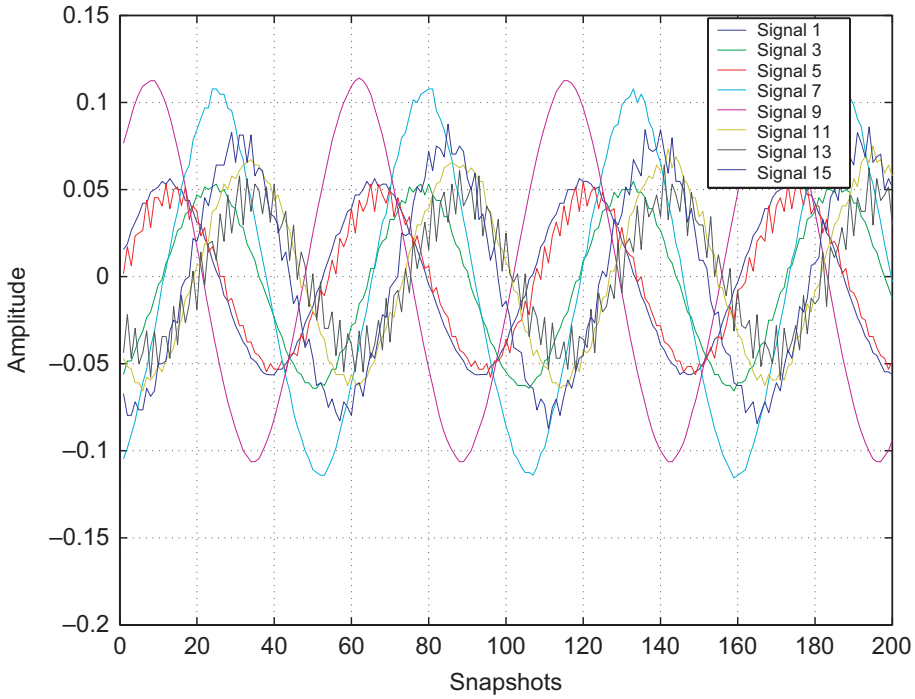

Fig. 10. The 8 uncalibrated in-line (I-branch) signals with a source at 0°.

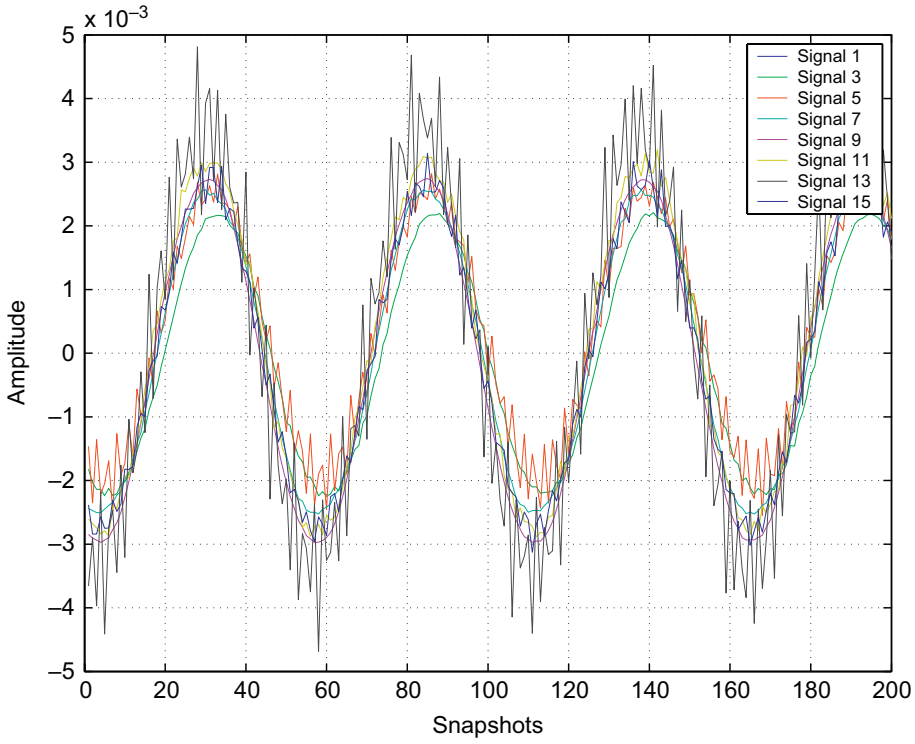

Fig. 11. The 8 calibrated in-line (I-branch) signals with a source at 0°.

These results are presented in Fig. 14. We can conclude that the performance of all these trained algorithms is much poorer when the training set is smaller (as usual) and the best tradeoff between performance and ease of implementation is provided by ADALINE.

A neural networks comparison based on their size follows in Table 1. In summary, the size of the

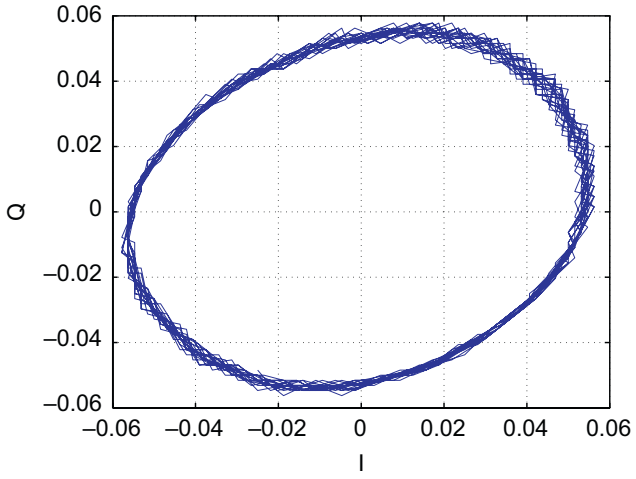

Fig. 12. Lissajou plot of antenna 1's in-line (I) and quadrature (Q) signals.

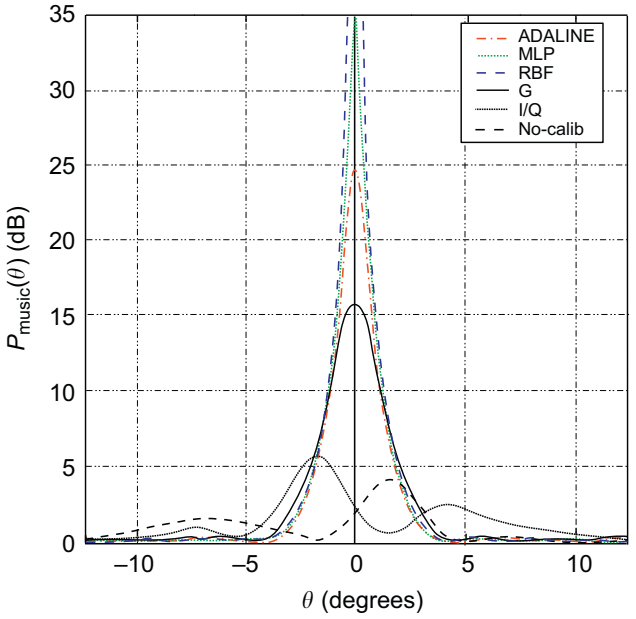

Fig. 13. Pseudospectrum obtained by MUSIC algorithm with calibrated and uncalibrated data of a source at 0°.

ADALINE network depends only on the number of antennas N; the RBF network depends on the number of antennas N and the size of the training set L; the size of the second layer of the MLP network depends on the number of antennas N and the first layer can be of any size, but empirically we conclude that to obtain good results, we have to fix this first layer the same size as the second one.

To demonstrate the good generalization capacity of the neural networks, they were used to calibrate new experimental steering vectors from the spatial covariance data matrix of two uncorrelated sources.

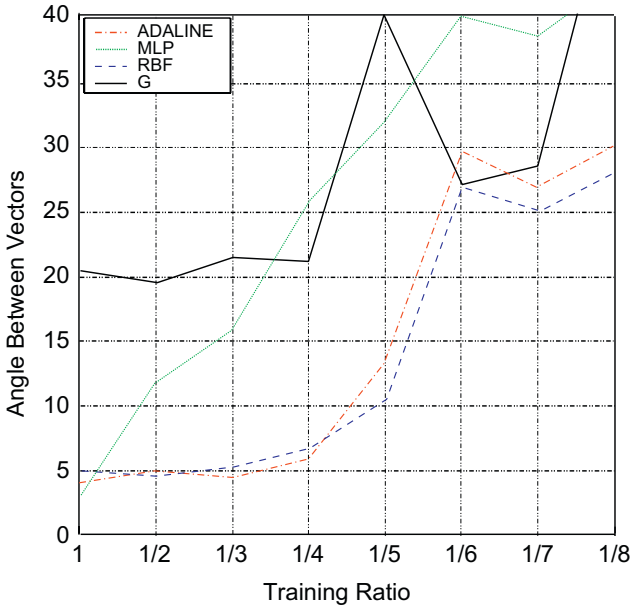

Fig. 14. Angle between calibrated and theoretical steering vectors for training set sizes. A unit training ratio implies a half-degree grid, while a training ratio of $\frac{1}{N}$ implies an $\frac{N}{2}$ degree grid, i.e. one out of N training positions are retained from the original grid.

Table 1
Neural networks size comparison

	$\mathbf{W}^1$	$\mathbf{b}^1$	$\mathbf{W}^2$	$\mathbf{b}^2$
ADALINE	$2N \times 2N$	$2N \times 1$	–	–
RBF	$L \times 2N$	$L \times 1$	$2N \times L$	$2N \times 1$
MLP	$2N \times 2N$	$2N \times 1$	$2N \times 2N$	$2N \times 1$

The results of two independent experiments obtained with the neural networks are compared in Figs. 15 and 16 with the same obtained with the method of the calibration matrix $\hat{\mathbf{G}}$ in (21).

The experiments are limited to two typical trials with two sources and the results are sufficiently satisfactory for our purposes: we can see in Figs. 15 and 16 that the proposed technique based on ADALINE generalizes well and outperforms the $\mathbf{G}$ matrix method while its computational complexity is of the same order. But the two other types of neural networks, MLP and RBF, are less attractive due to the presence of more peaks in the pseudospectrum than the real number of sources as can be seen in Figs. 15(a) and 16(a).

This can be explained given the fact that the training of a neural network can be seen as a function approximation of the input vectors. Hence, neural networks with too many degrees of freedom are probably too non-linear for this application and

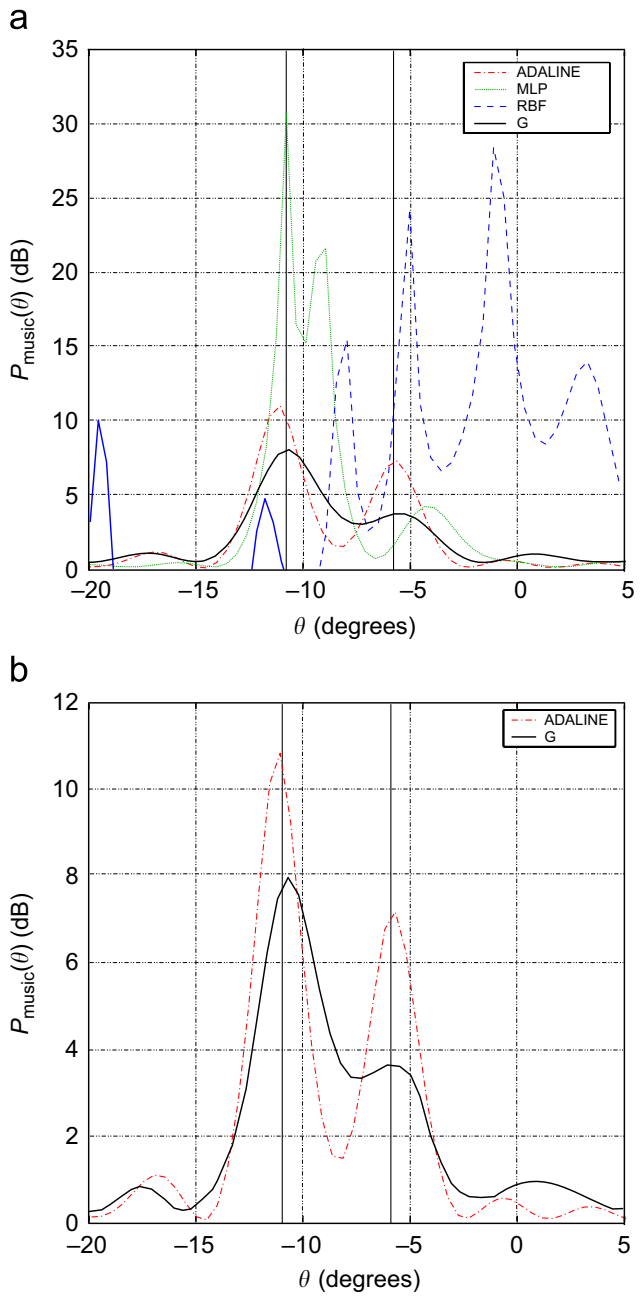

Fig. 15. Pseudospectrum obtained via the MUSIC algorithm with calibrated data of uncorrelated sources at -11° and -6° using various calibration techniques: (a) all techniques, (b) two best techniques only (ADALINE and G matrix).

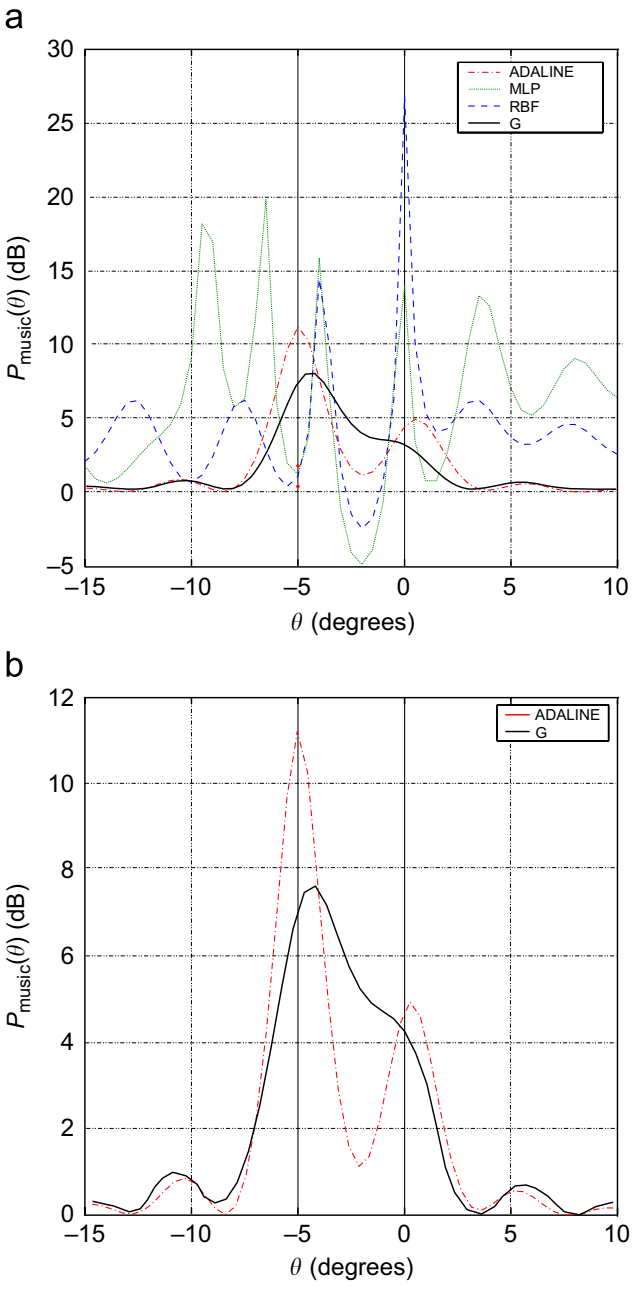

Fig. 16. Pseudospectrum obtained via the MUSIC algorithm with calibrated data of uncorrelated sources at -5° and -0° using various calibration techniques: (a) all techniques, (b) two best techniques only (ADALINE and G matrix).

will introduce unnecessary features, like curve fitting with a high-degree polynomial.

6. Conclusion

An original calibration technique based on neural networks was presented herein, trained by theoretical and experimental steering vectors. We find that the ADALINE neural network provides better—or very similar—results on average than all the other types of calibration techniques while being easy to implement in real-time. After many experimental trials it seems to always converge experimentally to the global minimum. The two other types of neural networks seem to be too non-linear for this problem, while being 1—longer to train (MLP) or 2—having many more neurons (RBF). Also, experiments have shown that branch-to-branch errors are

more critical for the performance of DOA algorithms than the I/Q one in an experimental context.

Moreover, the real-time capacity of the better algorithm, based on ADALINE neural networks, will be tested with a VLSI implementation with a new setup currently being developed comprising 3 antenna arrays of 8 elements equipped with FPGAs and DSPs for real-time signal processing. This new setup will allow us to obtain more results in different cases (e.g. various antenna array configurations, training grids with different angular spacings, etc.) to generalize the behavior of the algorithm facing the selection of different parameters and derive practical insights with respect to the desired resolution and the variability of the array response in certain specific directions. Also, a more exhaustive study implying Monte Carlo simulations will permit us to obtain the performance statistics and compare them with other calibration methods.

References

[1] A. Sinsky, P. Wang, Error analysis of a quadrature coherent detector processor, IEEE Trans. Aerospace Electronics Systems 10 (6) (November 1974) 880–883.

[2] N. Barber, Narrow band-pass filter using modulation, Wireless Eng. (May 1947) 132–134.

[3] N. Goodman, Statistical analysis based on a certain multivariate complex Gaussian distribution, Ann. Math. Stat. 34 (1963) 152–177.

[4] H. Park, S. Bang, Model based antenna array calibration for digital beamforming systems, in: Vehicular Technology Conference Proceedings, vol. 2, IEEE, April 2003, pp. 867–870.

[5] J. Pierre, R. Pappu, R. Kubichek, Effects of quadrature receiver gain error on direction-finding algortihms, in: Conference on Communications, Computers and Signal Processing, vol. 2, IEEE, May 1993, pp. 378–381.

[6] Y.-M. Chen, J.-H. Lee, C.-C. Yeh, J. Mar, Bearing estimation without calibration for randomly perturbated arrays, IEEE Trans. Signal Process. 39 (1) (January 1991) 194–197.

[7] M. Suk, S. Cho, K. Lee, J. Chun, A new calibration algorithm for cellular CDMA antenna arrays, in: Vehicular Technology Conference Proceedings, vol. 1, IEEE, September 2002, pp. 266–269.

[8] C. Lee, J. Chun, A subspace-based online calibration algorithm for an asynchronous CDMA-based antenna array, in: National Aerospace and Electronics Conference Proceedings, IEEE, October 2000, pp. 146–150.

[9] E. Hung, Matrix-construction calibration method for antenna arrays, IEEE Trans. Aerospace Electronics Systems 36 (3) (July 2000) 819–828.

[10] B. Friedlander, A. Weiss, Eigenstructure methods for direction finding with sensor gain and phase uncertainties, in: International Conference on Acoustics, Speech and Signal Processing, vol. 5, April 1988, pp. 2681–2684.

[11] B. Friedlander, A. Weiss, Direction finding in the presence of mutual coupling, IEEE Trans. Antennas Propag. 39 (3) (March 1991) 273–284.

[12] D. Fuhrmann, Estimation of sensor gain and phase, IEEE Trans. Signal Process. 42 (1) (January 1994) 77–87.

[13] C.-Y. Tseng, D. Feldman, L. Griffiths, Steering vector estimation in uncalibrated arrays, IEEE Trans. Signal Process. 43 (6) (June 1995) 1397–1412.

[14] J. Pierre, M. Kaveh, Experimental performance of calibration and direction-finding algorithms, in: International Conference on Acoustics, Speech and Signal Processing, vol. 2, April 1991, pp. 1365–1368.

[15] A. Weiss, B. Friedlander, Array shape calibration using sources in unknown locations—a maximum likelihood approach, IEEE Trans. Acoust. Speech Signal Process. 37 (12) (December 1989) 1958–1966.

[16] E. Hung, A critical study of a self-calibrating direction-finding method for arrays, IEEE Trans. Signal Process. 42 (2) (February 1994) 471–474.

[17] S. Kobayakawa, M. Tsutsui, Y. Tanaka, A blind calibration method for an adaptive array antenna in DS-CDMA systems using an MMSE algorithm, in: Vehicular Technology Conference Proceedings, vol. 1, IEEE, May 2000, pp. 21–25.

[18] G. Whipple, C. Keller, K. Forsythe, Performance characterization of external array self-calibration algorithms using experimental data, in: Conference on Signals, Systems and Computers, vol. 1, October 2000, pp. 623–628.

[19] M. Ali, J. Gotze, R. Pauli, An algorithm for the calibration of sensor arrays with sensor gain and phase uncertainties, in: International Conference on Acoustics, Speech and Signal Processing, vol. 4, April 1993, pp. 121–124.

[20] M. Wylie, S. Roy, H. Messer, Joint DOA estimation and phase calibration of linear equispaced (LES) arrays, IEEE Trans. Signal Process. 42 (12) (December 1994) 3449–3459.

[21] I. Gupta, J. Baxter, S. Ellingson, H.-G. Park, H. Oh, M. Kyeong, An experimental study of antenna array calibration, IEEE Trans. Antennas Propag. 51 (3) (March 2003) 664–667.

[22] F. Churchill, G. Ogar, B. Thompson, The correction of I and Q errors in a coherent processor, IEEE Trans. Aerospace Electronics Systems 17 (1) (January 1981) 131–137.

[23] J. Pierre, D. Fuhrmann, Considerations in the autocalibration of quadrature receivers, in: International Conference on Acoustics, Speech and Signal Processing, vol. 3, May 1995, pp. 1900–1903.

[24] J. Pierre, R. Green, Maximum likelihood technique to quadrature parameter estimation, in: International Conference on Acoustics, Speech and Signal Processing, vol. 4, April 1994, pp. 561–564.

[25] R. Green, R. Anderson-Sprecher, J. Pierre, Quadrature receiver mismatch calibration, IEEE Trans. Signal Process. 47 (11) (November 1999) 3130–3133.

[26] Y. Rockah, P. Schultheiss, Array shape calibration using sources in unknown locations—part I: far-field sources, IEEE Trans. Acoust. Speech Signal Process. 35 (3) (March 1987) 286–299.

[27] R. Ertel, Z. Hu, J. Reed, Antenna array hardware amplitude and phase compensation using baseband antenna arrays outputs, in: Vehicular Technology Conference Proceedings, vol. 3, IEEE, May 1999, pp. 1759–1763.

[28] K. Dandekar, H. Ling, G. Xu, Smart antenna array calibration procedure including amplitude and phase mismatch and mutual coupling effects, in: IEEE International Conference on Personal Wireless Communications, December 2000, pp. 293–297.
[29] M. Wiegmann, Antenna array calibration employing calibration beacons and steering vector estimation, in: International Conference on Antennas and Propagation, vol. 1, April 2001, pp. 41–44.
[30] B. Ng, C. See, Sensor-array calibration using a maximum-likelihood approach, IEEE Trans. Antennas Propag. 44 (6) (June 1996) 827–835.
[31] W. Youn, C. Un, Eigenstructure method for robust array processing, IEEE Electron. Lett. 26 (10) (May 1996) 678–680.
[32] H. Park, J. Jung, H. Oh, M. Kyeong, Model based antenna array calibration for smart antenna arrays, Electron. Lett. 38 (15) (July 2002) 771–772.
[33] A.E. Zooghby, C. Christodoulou, M. Georgiopoulos, Performance of radial-basis function for direction of arrival estimation with antenna arrays, IEEE Trans. Antennas Propag. 45 (11) (November 1997) 1611–1617.
[34] H. Southall, J. Simmers, T. O'Donnell, Direction finding in phased arrays with a neural network beamformer, IEEE Trans. Antennas Propag. 43 (12) (December 1995) 1369–1374.
[35] C. Christodoulou, M. Georgiopoulos, Applications of Neural Networks in Electromagnetics, Artech House, 2001.
[36] E. Charpentier, J.-J. Laurin, An implementation of a direction-finding antenna for mobile communications using a neural network, IEEE Trans. Antennas Propag. 47 (7) (July 1999) 1152–1159.
[37] J. Niven, K. Teague, Representation of antenna calibration data using modular neural networks, in: Symposium on Circuits and Systems, vol. 3, August 2002, pp. 117–120.
[38] S. Haykin, Adaptive Filter Theory, Prentice-Hall, Englewood Cliffs, NJ, 1996.
[39] J. Chang, Q. Wu, J.P. Reilly, A neural structure for direction finding with sensor array uncertainties, in: International Conference on Acoustics, Speech and Signal Processing, 1993.
[40] R. Schmidt, Multiple emitter location and signal parameter estimation, IEEE Trans. Antennas Propag. 34 (3) (March 1986) 276–280.
[41] M. Hagan, H. Demuth, M. Beale, Neural Networks Design, PWS Publishing Co., 1995.
[42] S. Haykin, Neural Networks: A Comprehensive Foundation, second ed., Prentice-Hall, Englewood Cliffs, NJ, 1999.
[43] H. Demuth, M. Beale, Neural Network Toolbox User's Guide, The Mathworks Inc., 2002.
[44] Y. Chen, W. du Plessis, Neural network implementation on a FPGA, in: Africon Conference in Africa, vol. 1, IEEE, 2002, pp. 337–342.
[45] Q. Wang, B. Yi, Y. Xie, B. Liu, The hardware structure design of perceptron with FPGA implementation, in: International Conference on Systems, Man and Cybernetics, vol. 1, IEEE, 2003, pp. 762–767.
[46] M. Vidal, D. Massicotte, A VLSI parallel architecture of a piecewise linear neural network for nonlinear channel equalization, in: Instrumentation and Measurement Technology Conference, vol. 3, IEEE, 1999, pp. 1629–1634.
[47] Wikipedia the free encyclopedia. ⟨http://en.wikipedia.org/wiki/Lissajouscurve⟩, 2007.